

- [9] a) B. Gates, Y. Yin, Y. Xia, *Chem. Mater.* **1999**, *11*, 2827. b) S. A. Johnson, P. J. Olivier, T. E. Mallouk, *Science* **1999**, *283*, 963. c) P. Jiang, J. Cizeron, J. F. Bertone, V. L. Colvin, *J. Am. Chem. Soc.* **1999**, *121*, 11 630. d) T. Casagneau, F. Caruso, *Adv. Mater.* **2002**, *14*, 34. e) D. Wang, F. Caruso, *Adv. Mater.* **2001**, *13*, 353. f) M. Deutsch, Y. A. Vlsou, D. J. Norris, *Adv. Mater.* **2000**, *12*, 1176.
- [10] Z. Zhong, Y. Yin, B. Gates, Y. Xia, *Adv. Mater.* **2000**, *12*, 206.
- [11] N. G. R. Broderick, G. W. Ross, H. L. Offerhouse, D. J. Richardson, D. C. Hanna, *Phys. Rev. Lett.* **2000**, *84*, 4345.
- [12] a) G. Decher, J. D. Hong, *Makromol. Chem. Macromol. Symp.* **1991**, *46*, 321. b) G. Decher, *Science* **1997**, *277*, 1232.
- [13] a) F. Caruso, R. A. Caruso, H. Möhwald, *Science* **1998**, *282*, 1111. b) E. Donath, G. B. Sukhorukov, F. Caruso, S. A. Davis, H. Möhwald, *Angew. Chem. Int. Ed.* **1998**, *37*, 2201.
- [14] For reviews, see: a) F. Caruso, *Chem. Eur. J.* **2000**, *6*, 413. b) F. Caruso, *Adv. Mater.* **2001**, *13*, 11.
- [15] F. Caruso, H. Lichtenfeld, E. Donath, H. Möhwald, *Macromolecules* **1999**, *32*, 2317.
- [16] a) G. Kumaraswamy, A. M. Dibaj, F. Caruso, *Langmuir* **2002**, *18*, 4150. b) Z. Liang, A. S. Susha, F. Caruso, *Adv. Mater.* **2002**, *14*, 1160.
- [17] It has been reported that the stoichiometry of lithium niobate is dependent on the Li:Nb molar ratio of the precursors used. Using LiNb(OC₂H₅)₆ with a Li:Nb molar ratio of 1:1 as a precursor leads dominantly to LiNbO₃ (S. Hirano, K. Kato, *J. Non-Cryst. Solids* **1988**, *100*, 538).
- [18] H. Fan, Y. Zhou, P. Lopez, *Adv. Mater.* **1997**, *9*, 728.
- [19] a) D. Wang, F. Caruso, *Chem. Mater.* **2002**, *14*, 1909. b) D. Wang, R. A. Caruso, F. Caruso, *Chem. Mater.* **2001**, *13*, 364.
- [20] K. Furusawa, W. Norde, J. Lyklema, *Kolloid Z. Z. Polymer* **1972**, *250*, 908.
- [21] H. Riegler, M. Engel, *Ber. Bunsen-Ges.* **1991**, *95*, 1424.
- [22] N. D. Denkov, O. D. Velev, P. A. Kralchevsky, I. B. Ivanov, H. Yoshimura, K. Nagayama, *Langmuir* **1992**, *8*, 3183.

Porous Polymer and Cell Composites That Self-Assemble In Situ**

By Aliasger K. Salem, Felicity R. A. J. Rose, Richard O. C. Oreffo, Xuebin Yang, Martyn C. Davies, John R. Mitchell, Clive J. Roberts, Snjezana Stolnik-Trenkic, Saul J. B. Tendler, Phil M. Williams, and Kevin M. Shakesheff*

An aim of tissue engineering is to regenerate tissues within a patient by delivering specific cells to a site of damage and then triggering their proliferation and differentiation.^[1] Examples of such applications include stem cell delivery to the spinal cord,^[2] bone defects,^[3] and the pancreas.^[4] A delivery vehicle is required for the cells that can fill the damaged space within the body and supply signals to cells. Ideally, the vehicle would have similar properties to the porous scaffolds that have proven successful in ex vivo regeneration of tissues such as cartilage,^[5] bone,^[6] and liver.^[7] Here we report a new porous scaffold that can be delivered by syringe into a tissue

[*] Prof. K. M. Shakesheff, Dr. A. K. Salem, Dr. F. R. A. J. Rose, Prof. M. C. Davies, Dr. C. J. Roberts, Dr. S. Stolnik-Trenkic, Prof. S. J. B. Tendler, Dr. P. M. Williams
School of Pharmaceutical Sciences, The University of Nottingham
Nottingham NG7 2RD (UK)
E-mail: kevin.shakesheff@nottingham.ac.uk
Dr. R. O. C. Oreffo, X. Yang
University Orthopaedics, University of Southampton
General Hospital, Southampton SO16 6YD (UK)
Prof. J. R. Mitchell
School of Biological Sciences, The University of Nottingham
Nottingham NG7 2RD (UK)

[**] The authors acknowledge the BBSRC and EPSRC for support.

or cavity as a polymer and cell slurry. Immediately following delivery, the slurry self-assembles into a porous scaffold with cells distributed throughout. Self-assembly involves the cross-linking of polymer particles by a mechanism that does not interfere with cell function.

In broad terms, tissue engineering scaffolds are either preformed water-insoluble matrices, with large interconnected pores within which cells are seeded, or hydrogels that solidify around the cell population.^[8,9] The matrix scaffold is formed before cells are seeded and then it is either placed in a bioreactor for in vitro tissue formation or implanted into a patient for augmented in vivo tissue regeneration. Whilst the three-dimensional cell culture environment within these porous scaffolds is favorable to tissue regeneration, the need to preform the scaffold before seeding and implantation is problematic. Cell seeding methods can be inefficient due to poor transport of the cells through the matrix and cell damage. In terms of implantation, the scaffold must be shaped to fill a cavity within the body, requiring knowledge of the cavity dimensions and an invasive operation. In contrast, a number of hydrogel materials have been designed that can be delivered directly into the body through a syringe. The gel forms within the body following a trigger signal, for example a temperature change or UV light exposure.^[10,11] Such systems have the advantage that they can fill cavities of any shape without prior knowledge of the cavity dimensions. However, such hydrogels lack large interconnected porous networks and, hence, tissue formation is limited by the barrier of diffusion to signaling and nutrient molecules.

Our novel material possesses features of both porous matrices and in situ forming gels to generate porous scaffolds that self-assemble at the site of injection, entrapping the delivered cells without compromising viability. Figure 1 is a schematic representation of the process of scaffold self-assembly. We start with particles of poly(lactic acid)-poly(ethylene gly-

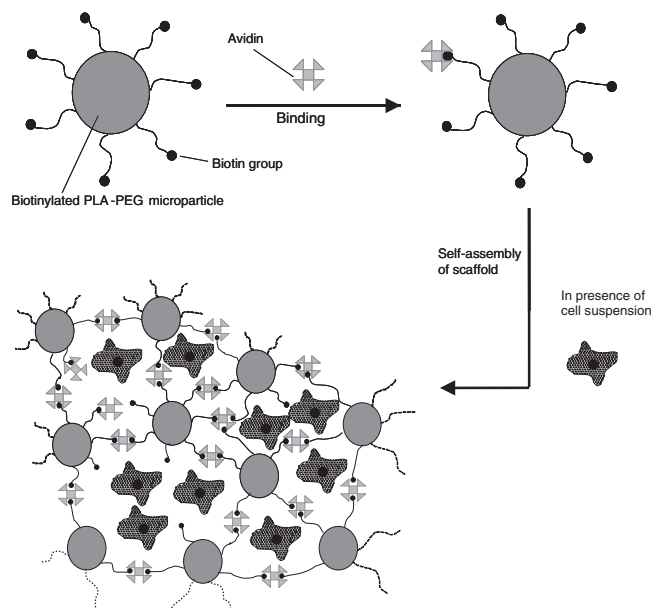


Fig. 1. A schematic representation of scaffold self-assembly.

col)-biotin (PLA-PEG-biotin)^[12] that are formed by conventional methods.^[13] These particles may be loaded with growth factors or other signaling molecules.^[14] The particles are mixed with a suspension of cells in an appropriate cell culture medium and then co-injected with the crosslinking protein, avidin. At specific concentrations of avidin, crosslinking of the microparticles occurs and a scaffold forms around the cells. Scaffold solidification begins within seconds of mixing of the components. Optionally, additional biotinylated molecules may be added to the initial particle/cell slurry. For example, we have shown that biotinylated peptides can be added to surface engineer the particles and promote integrin-mediated cell adhesion,^[12] or bifunctional PEG can be added to increase the gel-forming component in the scaffold.

The crosslinking of nano- and microparticles through the avidin bridges and the criticality of the avidin concentration was demonstrated by particle sedimentation and size data (Figs. 2A and 2B). At low avidin concentrations there are insufficient bridging points due to the scarcity of the protein. At high avidin concentrations there are insufficient free biotin molecules on the surfaces of the particles to achieve crosslinking. At intermediate avidin concentrations the probability of a surface-bound avidin molecule encountering a free biotin on a neighboring particle is maximized.

The mechanisms of self-assembly have further been explored by surface plasmon resonance (SPR) analysis and rheological measurement of the bridging process. The specific receptor-mediated nature of the crosslinking is demonstrated in the SPR data in Figure 2C. The silver-coated SPR slides were modified with a biotin-presenting monolayer by exposure to *N*-([6-biotinamido]-hexyl)-3'-[2'pyridylthio]propionamide. Successive layers of avidin, biotin-PEG-biotin, avidin, and PLA-PEG-biotin nanoparticles were then built upon this surface. The addition of each layer, via specific avidin-biotin interactions, was detected by an increase in the SPR angle. Rheologically, the scaffold displays viscoelastic liquid properties without the avidin crosslinking agent ($G'' > G'$). At optimum avidin concentrations, the scaffold behaves as a viscoelastic solid, i.e., the storage modulus is greater than the loss modulus over the whole frequency range (Fig. 2D).

Next, the self-assembly of three-dimensional porous scaffolds was demonstrated (Fig. 3). The scaffold shown in Figure 3A conformed to the pyramidal shape of the mold into which it was injected with the individual microparticles clustering to form a three-dimensional network around a cell population. In the absence of the crosslinker, the microparticle slurry failed to maintain the pyramidal shape on removal from the mould. The confocal fluorescence image in Figure 3B dis-

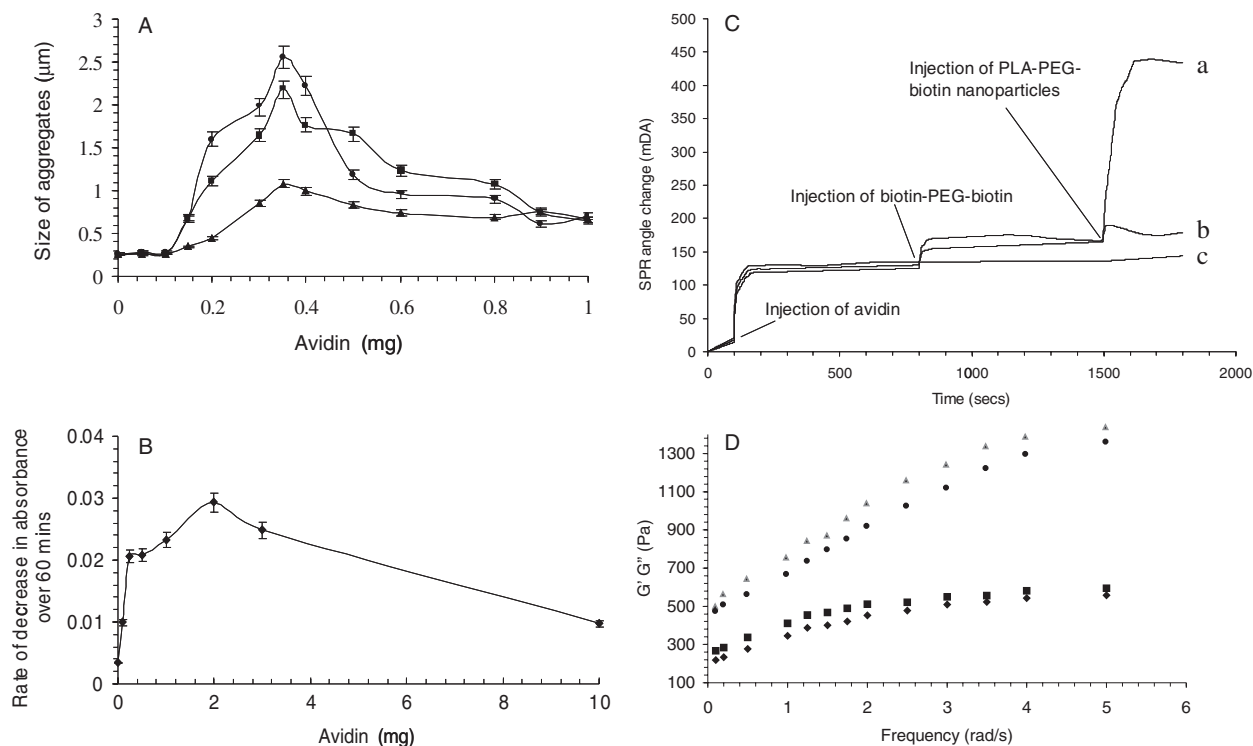


Fig. 2. Agglomeration of nano- and micro-PLA-PEG-biotin particles on the addition of avidin. A) Photon correlation spectroscopy (PCS) data on different dilutions of PLA-PEG-biotin nanoparticles with the addition of avidin to determine nanoparticle concentration and avidin-to-nanoparticle ratio effects on aggregation. 5 $\mu\text{g mL}^{-1}$ nanoparticles (\blacktriangle), 25 $\mu\text{g mL}^{-1}$ nanoparticles (\blacksquare), 50 $\mu\text{g mL}^{-1}$ nanoparticles (\bullet) B) Sedimentation studies, showing rate of decrease in absorbance for 10 mg mL^{-1} PLA-PEG-biotin particles ($\approx 10 \mu\text{m}$) with varying concentrations of avidin. C) SPR experiment to determine the rate of binding of avidin-saturated PLA-PEG-biotin nanoparticles with biotin-PEG-biotin. a) Spectrum for the injection of avidin, followed by the injection and binding of a biotin-PEG-biotin layer, and finally binding of nanoparticles saturated with avidin. Controls included b) the injection of nanoparticles without avidin saturation and c) avidin only. D) Mechanical spectra (elastic modulus G' and viscous modulus G'' versus frequency of applied strain) within the linear viscoelastic region. Comparison of viscoelastic properties of scaffold (50% PLA-PEG-biotin microparticles/25% PEG-biotin) at 37 $^{\circ}\text{C}$ with and without avidin treatment. G' no avidin (\blacklozenge), G'' no avidin (\blacksquare), G' avidin in saturated microparticles (\blacktriangle), G'' avidin in saturated microparticles (\bullet).

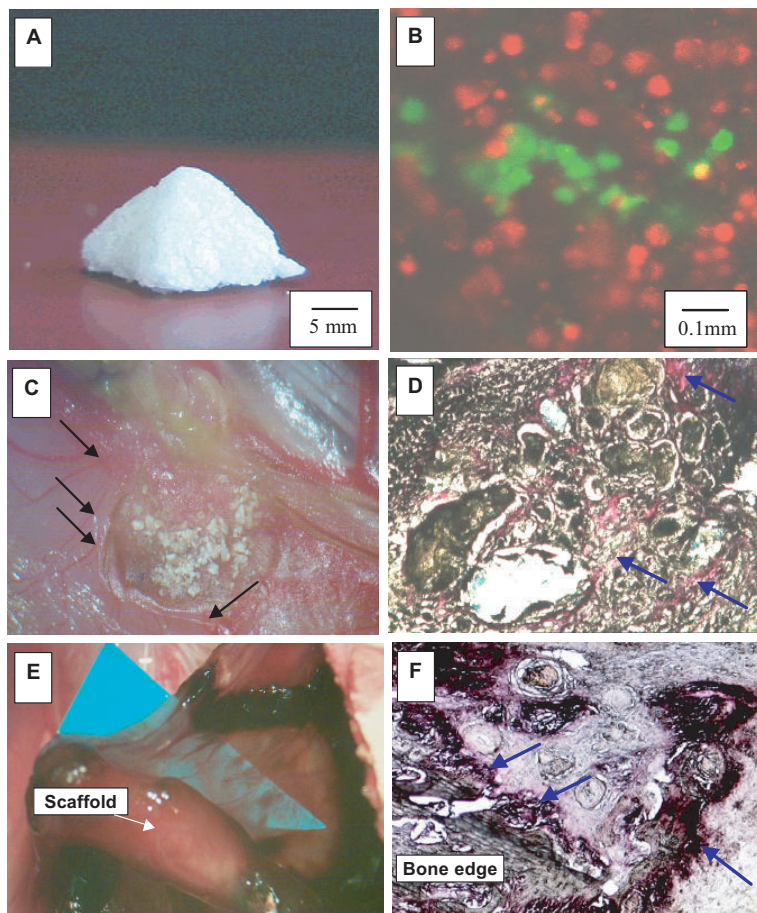


Fig. 3. A) PEG-biotin in poly(dimethylsiloxane) (PDMS) molds. B) Confocal microscopy images of cross sections of scaffold (red reflectance) displaying entrapped osteoblasts (green, CellTracker). C) In-situ photomicroscopy of porous scaffold after 7 days on CAM culture. The scaffold has remained aggregated, in situ, with extensive blood vessel invasion (arrows) from the CAM (magnification $\times 20$). D) Paraffin section ($5\ \mu\text{m}$) of (C) stained with alcian blue and sirius red, demonstrating CAM in-growth and matrix synthesis from CAM tissue (magnification $\times 50$). E) In-situ photomicroscopy of scaffold within chick femur defect after 7 days on CAM culture. Invasion of blood vessels (contrasted against blue paper) from CAM on and around the femur and scaffold can be observed (magnification $\times 10$). Explant-scaffold constructs were placed in CAM culture for 7 days. F) Paraffin section of scaffold within the femur wedge defect from (E) stained for alkaline phosphatase activity. Alkaline phosphatase activity of CAM tissue and at the cut bone edge integrated with the scaffold can be observed (magnification $\times 50$). Blue arrows indicate examples of regions of contact between the existing bone and the scaffold where new tissue formation has occurred.

plays the distribution of a human osteoblast sarcoma cell population through a section of the scaffold with the cells identified by a fluorescent marker (green/excitation 488 nm) and the PLA-PEG-biotin microparticles identified by the reflected light signal (red/RT 30:70). Confocal images were taken throughout the scaffold and displayed single cells and small clusters of cells distributed evenly. Confocal microscopy also revealed a porous structure created by the imperfect packing of the microparticles. Pores with diameters in the range of 5 to 20 μm formed within clusters of microparticles. Between clusters, larger pores of up to 100 μm were observed.

The chorioallantoic membrane (CAM) of growing chick embryos has been widely used as an assay system for angiogenesis and as an explant tissue culture system.^[15] Initially we examined the toxicity of the porous scaffold within this angio-

genic assay. Porous scaffolds were injected dropwise onto the surface of the CAM of day 10 chick embryos. After 7 days, widespread vascularization across the porous scaffold (Fig. 3C) was observed with invasion of blood vessels from the CAM into the scaffold. Extensive matrix formation of proteoglycan and collagen by the invading CAM was confirmed by alcian blue and sirius red staining (Fig. 3D). As a final proof-of-concept, we have modified this system to demonstrate, ex vivo, the biological compatibility of the porous polymer scaffold on live chick bones and to illustrate the potential application to fill a bone defect using this technology. Wedge-shaped bone defects were prepared from femurs isolated from day 18 chick embryos, under a dissecting microscope. The defects were then filled with cell-free scaffold and cultured for a further 7 days on the CAM. As shown in Figure 3E, pervasive vascularization from the CAM to the chick femur/scaffold construct was observed. The demonstration of alkaline phosphatase staining confirmed the viability of the bone and close integration of the scaffold to the chick bone and CAM without loss of viability (Fig. 3F).

The novel molecular-interaction mechanism of self-assembly of these scaffolds differentiates this material from other injectable systems. The formation of porous scaffolds within a cavity or a soft tissue could be a prerequisite for tissue remodeling using new cell sources such as stem cells. Improvements in the control of porosity and potential problems with avidin immunogenicity may need to be addressed for certain tissue engineering applications. The basic component of the scaffold is a biodegradable microparticle that can be formed from any of the poly(α -hydroxyacids) or indeed other polymers. Hence, conventional controlled release technologies and surface engineering can be combined with the self-assembly to form biomimetic scaffolds that stimulate integrin-mediated cell adhesion and then release growth factors.

Experimental

Preparation of PLA-PEG-Biotin: This is described in detail in the literature [12].

Preparation of Biotin-PEG-Biotin: α - ω -bis(amine) PEG (1 g) was dissolved in acetonitrile (2 mL), methylene chloride (1 mL), Et_3N (80 μL), and NHS-Biotin (0.50 g). The reactants were stirred overnight under argon and then worked up using diethyl ether (40 mL) to precipitate the polymer. The isolated material was then dissolved in hot isopropanol (70 $^\circ\text{C}$) to give an opaque-cloudy solution. On cooling the product was filtered and lyophilized.

Preparation of Nano/Microparticles: 500 mg of PLA-PEG-biotin was dissolved in 20 mL of dichloromethane (DCM) to produce a 25 mg mL^{-1} solution. Poly(vinyl alcohol) (PVA) (M_w 250 000) [88% hydrolyzed] was dissolved into distilled water (0.1% w/v solution). The PLA-PEG-biotin solution was then added to a PVA solution. The mixture was homogenized for a further 10 min at 5000 rpm and then left stirring overnight to allow the DCM to evaporate and microparticles to form. The average microparticle diameter was 9.9 μm (poly-

dispersity 0.29) measured using a Coulter LS230. Nanoparticles were prepared as above with a 9% w/v PVA solution, homogenization at 5000 rpm and a 5 mg mL⁻¹ solution of PLA-PEG-biotin. The average nanoparticle diameter was 250 nm (polydispersity 0.55) measured using a Coulter LS230.

Surface Plasmon Resonance (SPR): The SPR equipment (Ortho Clinical Diagnostics, Chalfont, St-Giles, UK) employs a Kretschmann configuration with a monochromatic laser source of 780 nm wavelength and silver-coated glass slides biotinylated by incubating in a 0.1 mg mL⁻¹ solution of *N*-([6-biotin-amido]hexyl)-3'-[2'-pyridylthio]propionamide in trifluoroethanol (TFE). PLA-PEG-biotin nanoparticles (250 nm) were saturated in excess avidin and washed using centrifugation. The avidin-saturated nanoparticles (1.5 × 10⁻⁷ M) were then prepared in 10 mM sodium phosphate buffer (pH 7.4). For the purposes of a stable baseline reading, a sodium phosphate buffer wash (10 mM, pH 7.4) was first passed over the biotin-HPDP (*N*-([6-biotinamido]hexyl)-3'-[2'-pyridylthio]propionamide) functionalized surface for 100 s. Avidin-functionalized surfaces were then obtained by flowing avidin solution (1.5 × 10⁻⁷ M) over the biotinylated slides. To remove any excess avidin, sodium phosphate buffer (10 mM, pH 7.4) was then washed over the surface. Then biotin-PEG(3350)-biotin (1 × 10⁻⁶ M) was flowed across the sample surface, followed by a buffer wash. Avidin-saturated nanoparticles (1.5 × 10⁻⁷ M) were then flowed over the surface followed by a buffer wash. As a control experiment, unsaturated PLA-PEG-biotin nanoparticles (1.5 × 10⁻⁷ M, 250 nm) were injected in place of the avidin-saturated nanoparticles following the avidin and biotin-PEG-biotin injections. A further control involved injecting avidin alone over the experimental time period. The flow rate was 0.24 mL min⁻¹ with results taken from at least 8 repeats. The change in the SPR angle was monitored over time in units of millidegrees angle (mDA) where 1 mDA = 0.001°.

Oscillatory Shear Measurements: Oscillatory shear measurements were performed using a controlled stress rheometer (CS10, Bohlin) fitted with a cone and plate (4° geometry) and used a frequency range of 0.1–5 rad s⁻¹ at 37 °C. The linear viscosity region (where stress is proportional to strain) was determined by stress sweep measurements in order to carry out measurements at stresses that did not damage the scaffold structure.

Cell Culture Experiments: Human Osteoblast Sarcoma (HOS) cells were cultured in Dulbecco's Modified Eagle's Medium (DMEM) supplemented with 10% fetal calf serum (FCS), 2 mM L-glutamine, 100 U mL⁻¹ penicillin, 100 µg mL⁻¹ streptomycin and 0.25 µg mL⁻¹ amphotericin B (antibiotic/antimycotic), 1 × non-essential amino acids (NEAA), and 75 mg ascorbic acid. Cell cultures were incubated at 37 °C in a 5% CO₂ enriched atmosphere. Every 2–3 days the cells were passaged, using 0.25% trypsin/1 mM ethylenediaminetetraacetic acid (EDTA) in phosphate buffered saline (PBS), and reseeded. Cells were incubated with Cell Tracker green 5-chloromethylfluorescein diacetate (CMFDA) fluorescent stain (Molecular Probes), by reconstituting the material in 11 µL dimethylsiloxane (DMSO) and adding this solution to the media of a confluent monolayer of cells for 45 min. The medium was then replaced and the cells incubated for a further hour. Following trypsinization and resuspension, the cells were centrifuged and resuspended in DMEM. Approximately 1 × 10⁶ cells were placed into a mixture of 50% avidin-saturated PLA-PEG-biotin microparticles and 25% biotin-PEG-biotin was added to this to aggregate the microparticles and entrap the cells. Scaffolds were examined using a confocal microscope.

Chorioallantoic Membrane Culture: Fertilized eggs were incubated for 10–18 days using a Multihatch automatic incubator (Brinsea Products, Sandford, UK) at 37 °C in a humidified atmosphere. On day 10, eggs were removed and a 1 cm² square section cut into the shell. Scaffolds were injected dropwise directly onto the CAM of 10 day old chick embryos and incubation continued for a further 7 days. In addition, femurs were excised from day 18 chick embryos and a wedge-shaped segmental defect created in the middle of the femur, into which the scaffold was injected to fill the defect site. The femoral/scaffold explant was then placed onto the CAM and incubation, at 37 °C, continued for a further 7 days as previously detailed [15]. Explants were then harvested and the chick embryo killed by decapitation. Prior to histochemical analysis, scaffold and explant samples were fixed in 95% ethanol, processed to paraffin wax, and 5 µm sections prepared. Sections were stained with alcian blue/sirius red and alkaline phosphatase to demonstrate proteoglycan, collagen, and enzyme activity as follows:

i) **Alkaline Phosphatase Activity:** Samples were stained using a Sigma alkaline phosphatase kit (no.85).

ii) **Alcian Blue/Sirius Red:** Samples were stained using Weigert's hematoxylin, alcian blue (in 1% acetic acid) and sirius red (in saturated picric acid).

Received: July 26, 2002

Final version: November 19, 2002

- [1] L. G. Cima, J. P. Vacanti, C. Vacanti, D. Ingber, D. Mooney, R. Langer, *J. Biomech. Eng.* **1991**, *113*, 143.
[2] J. W. McDonald, X. Z. Liu, Y. Qu, S. Liu, S. K. Mickey, D. Turetsky, D. I. Gottlieb, D. W. Choi, *Nature Med.* **1999**, *5*, 1410.

- [3] R. O. C. Oreffo, J. T. Triffitt, *Bone* **1999**, *25*, 5S-9S.
[4] V. K. Ramiya, M. Maraist, K. E. Arfors, D. A. Schatz, A. B. Peck, J. G. Cornelius, *Nature Med.* **2000**, *6*, 278.
[5] R. G. LeBaron, K. A. Athanasiou, *Biomaterials* **2000**, *21*, 2575.
[6] D. W. Hutmacher, *Biomaterials* **2000**, *21*, 2529.
[7] L. G. Cima, D. E. Ingber, J. P. Vacanti, R. Langer, *Biotechnol. Bioeng.* **1991**, *38*, 145.
[8] K. J. L. Burg, W. D. Holder, C. R. Culberson, R. J. Beiler, K. G. Greene, A. B. Loebbeck, W. D. Roland, P. Eiselt, D. J. Mooney, C. R. Halberstadt, *J. Biomed. Mater. Res.* **2000**, *51*, 642.
[9] C. K. Kuo, P. X. Ma, *Biomaterials* **2001**, *22*, 511.
[10] B. Jeong, Y. H. Bae, D. S. Lee, S. W. Kim, *Nature* **1997**, *388*, 860.
[11] J. Elisseeff, W. McIntosh, K. Anseth, S. Riley, P. Ragan, R. Langer, *J. Biomed. Mater. Res.* **2000**, *51*, 164.
[12] S. M. Cannizzaro, R. F. Padera, R. Langer, R. A. Rogers, F. E. Black, M. C. Davies, S. J. B. Tendler, K. M. Shakesheff, *Biotechnol. Bioeng.* **1998**, *58*, 529.
[13] S. M. Howdle, M. S. Watson, M. J. Whitaker, V. K. Popov, M. C. Davies, F. S. Mandel, J. D. Wang, K. M. Shakesheff, *Chem. Commun.* **2001**, 109.
[14] J. E. Babensee, L. V. McIntire, A. G. Mikos, *Pharm. Res.* **2000**, *17*, 497.
[15] H. I. Roach, J. E. Baker, N. M. P. Clarke, *J. Bone Miner. Res.* **1998**, *13*, 950.

Improved Crystal-Growth and Emission Gain-Narrowing of Thiophene/Phenylene Co-Oligomers**

By Musubu Ichikawa,* Ryota Hibino, Masamitsu Inoue, Takeshi Haritani, Shu Hotta, Toshiki Koyama, and Yoshio Taniguchi

Unique optoelectronic features have been demonstrated using molecular semiconductors in (poly)crystalline phases. Examples include lasing and amplified spontaneous emission (ASE) from acene-, phenylene-, or thiophene-based materials that are photoexcited or charge-injected through electrodes on suitably constructed devices. Accordingly, crystals of high quality are increasingly needed to achieve high optoelectronic performance.

To this end, various crystal-growth techniques have been proposed and developed to date. As a typical example, single crystals of, for example, anthracene or naphthalene were made via well-established techniques, such as the zone-melting method and the Bridgman method. More recently, Kloc et al. proposed a crystal-growth method in the vapor phase under a considerably high pressure of environmental gas (such as argon, helium, and hydrogen).^[1,2] That method made accessible large single crystals of molecular materials. For instance,

* Dr. M. Ichikawa, R. Hibino, Dr. M. Inoue, T. Haritani, Dr. T. Koyama, Prof. Y. Taniguchi
Department of Functional Polymer Science
Faculty of Textile Science and Technology, Shinshu University
Tokita 3-15-1, Ueda, Nagano 386-8567 (Japan)
E-mail: musubu@giptc.shinshu-u.ac.jp

Dr. S. Hotta
Photonics and Materials Research Department
Institute of Research and Innovation, Kashiwa Laboratory
1201 Takada, Kashiwa, Chiba 277-0861 (Japan)

** This work was supported by the New Energy and Industrial Technology Development Organization (NEDO) for Organic Materials Technology for a Solid-State Injection Laser theme. This work was also supported by a Grant-in-Aid for COE Research (10CE2003) from the Japanese Ministry of Education, Culture, Sports, Science, and Technology.